

Optimization of the Electrospinning Conditions by Box-Behnken Design to Prepare Poly(Vinyl Alcohol)/Chitosan Crosslinked Nanofibers

Vinícius R. Viana^{1*}, Willian H. Ferreira¹, Edwin G. Azero², Marcos L. Dias¹, Cristina T. Andrade¹

¹Instituto de Macromoléculas Professora Eloisa Mano, Universidade Federal do Rio de Janeiro, Centro de Tecnologia, Bloco J, Rio de Janeiro, Brazil

²Departamento de Ciências Naturais, Universidade Federal do Estado do Rio de Janeiro, Avenida Pasteur, Rio de Janeiro, Brazil

Email: *vianavr@ima.ufrj.br

How to cite this paper: Viana, V.R., Ferreira, W.H., Azero, E.G., Dias, M.L. and Andrade, C.T. (2020) Optimization of the Electrospinning Conditions by Box-Behnken Design to Prepare Poly(Vinyl Alcohol)/Chitosan Crosslinked Nanofibers. *Journal of Materials Science and Chemical Engineering*, 8, 13-31.

<https://doi.org/10.4236/msce.2020.84002>

Received: March 19, 2020

Accepted: April 17, 2020

Published: April 20, 2020

Copyright © 2020 by author(s) and Scientific Research Publishing Inc.

This work is licensed under the Creative Commons Attribution International License (CC BY 4.0).

<http://creativecommons.org/licenses/by/4.0/>



Open Access

Abstract

Electrospun poly(vinyl alcohol)/chitosan nanofibers had their solution and process parameters optimized using a Box-Behnken design and desirability function. Four factors (applied voltage, flow rate, distance tip-to-plate and amount of chitosan) were varied to produce electrospun mats with a low fiber diameter. An empirical model was developed for each response using response surface methodology (RSM), which revealed that flow rate had no significant influence on the assessed responses. With desirability function, the optimal conditions to produce the nanofibers were applied voltage of 13.1 kV, 30% chitosan concentration and distance tip-to-plate of 10 cm. The fiber diameter and standard deviation were 196.5 ± 28.3 nm, compared to the predicted values of 185.9 ± 26.8 nm. The desirability function allied with Box-Behnken design proved themselves important tools to predict process parameters for the development of nanofibers. The mats were crosslinked with glutaraldehyde for 24 h and 48 h and presented good water stability and enhanced mechanical properties.

Keywords

Electrospinning, Poly(Vinyl Alcohol), Chitosan, Box-Behnken Design

1. Introduction

Electrospinning is a promising and versatile technique that is used to fabricate polymeric nanofibers for a wide variety of biomedical applications such as drug delivery systems [1], scaffolds for tissue engineering [2] [3] [4] [5], wound

dressing [6]. Fibers produced by electrospinning have controlled dimensions, about a few nanometers, and porosity, which give the produced fibers a high surface area [5] [7]. Achieving these characteristics depends on a wide range of factors such as solution parameters (polymer concentration, conductivity and viscosity), process-related parameters (polymer flow rate, distance tip-to-plate, and applied voltage), as well as humidity and temperature [1] [5]. Due to the inherent properties of the electrospinning process, the arrangement of polymeric fibers can be controlled with the aim of obtaining complex and three-dimensional nanofibers. In addition, depending on the polymer used, a wide range of properties such as strength, porosity, functionalized surface may be achieved [8] [9]. Furthermore, the electrospinning process allows the spinning of a wide variety of polymers, natural or synthetic, such as the combination of these polymers.

Chitosan (CS) is composed of repeating units of 2-acetamido-2-deoxy-D-glycopyranose (N-acetylglucosamine) joined by β -(1 \rightarrow 4) bonds. This biopolymer has characteristics such as hydrophilicity, biodegradability, biocompatibility and low toxicity [10]. In addition, it does not cause allergic reactions or rejection problems, has bioadhesive properties, increases the residence time of chitosan-based systems at specific absorption sites, controlled release and improved bioavailability, and has antimicrobial activity [11] [12]. Due to these characteristics, chitosan can be considered a promising biomaterial, which can be used for the preparation of several drug delivery systems, including nanofibers [13] [14] [15] [16]. In studies involving the use of chitosan as biomaterial, in addition to mechanical properties, chondrocyte proliferation and extracellular matrix production, such as glycosaminoglycans and type I and type II collagen, were verified. Such information reinforces that chitosan can be a potential biomaterial for tissue engineering, including the production of nanofibers for topical drug administration [17] [18] [19] [20] [21]. However, chitosan is not soluble in organic solvents, and its aqueous solutions are not electrospinnable. To overcome this problem, CS dissolved in acidic aqueous solution is mixed with nonionic polymer solutions such as poly(vinyl alcohol) (PVA) improving the viscoelastic properties and the electrospinnability of the CS solution [22].

PVA is a chemically stable water soluble, non-toxic, biocompatible and biodegradable polymer with good film and fiber forming properties [23] [24]. Because of its characteristics, this polymer stands out in several biomedical applications, such as tissue regeneration, modified drug release system or hydrogels. PVA also stands out for being used in electrospinning, producing regular fibers of good morphology on the nanometer scale [25] [26] [27]. Although the production of biomaterials involving PVA/CS blends has already been studied, there are few studies that relate the influences of process parameters to the materials produced by electrospinning with PVA/CS. In this context, the application of statistical methods of design of experiments (DoE) to obtain mathematical models sheds new light on the electrospun PVA/CS nanofibers.

Mathematical tools have been widely used in recent years in order to find relationships between the variables of a study by multivariate statistical techniques.

The aim of DoE is to maximize or minimize the responses of interest using a small number of experiments even with a wide range of factors [28]. Box-Behnken is a design used for the adjustment of quadratic functions. It is considered an economical and efficient tool for determining first and second order coefficients of regression models [29]. BBD is a 3-level (3k) statistical design where k is the number of factors to be tested. Its experimental matrix eliminates the vertices points of a cube and it is not possible to carry out experiments under extreme conditions. In other words, it is not possible to perform an experiment with all factors at the maximum or minimum level simultaneously, which may prove to be an advantage in some cases [30] [31]. Its experimental matrix eliminates the vertices points of a cube and it is not possible to carry out experiments under extreme conditions, that is, all factors at the maximum or minimum level simultaneously, which may prove to be an advantage in some cases [30] [31]. The use of Box-Behnken design in the production of nanofibers has been reported by several authors in order to understand the influence of solution and process parameters on the formation of materials, as well as the optimization of significant factors [32] [33] [34] [35].

Response Surface Methodology (RSM) is a mathematical technique that, when allied with DoE, is ideal for constructing models and find optimal conditions for one or more responses. One of the main advantages of RSM is the ability to exclude insignificant factors and interactions from the regression model [28] [31] [36]. In situations where the best conditions of a process are to be determined, the desirability method becomes a very useful tool for the simultaneous optimization of multiple responses. Thus, it is possible to obtain the best conditions of the multiple independent variables simultaneously, both to maximize and to minimize or even to obtain specific nominal values [37] [38]. For this, the expected result will depend on the desired objective (maximization, normalization or minimization), the specified limits and the weight assigned to each of the responses [39].

This work aims to investigate the influence of process parameters on the morphology of PVA/CS electrospun nanofibers. A four-factor three-level Box-Behnken design was used to determine the better conditions of electrospinning processing to optimize the production of PVA/CS nanofibers.

2. Materials and Methods

2.1. Materials

Poly(vinyl alcohol) (PVA) was supplied by Vetec Química Fina (Rio de Janeiro, RJ, Brazil) with molecular weight of 85,300 g/mol and 88% degree of hydrolysis. Medium molecular weight chitosan (CS), degree of acetylation (DA = 15%) and the viscosity-average molecular weight ($\bar{M}_v = 296772$), and glutaraldehyde were provided by Sigma Aldrich (São Paulo, SP, Brazil). Analytical grade acetic acid was purchased from Vetec Química Fina Ltda. (Rio de Janeiro, RJ, Brazil). All materials were used without previous purification.

2.2. Nanofiber Development

2.2.1. Preparation of Solutions

PVA and CS stock solutions were prepared in ultrapure water (Milli-Q) and 2% (v/v) acetic acid solution, respectively, under constant stirring for 16 h. In this study, the concentration of PVA was set at 10% (w/v), whereas that of CS was set at 2.5% (w/v). Appropriate quantities of each solution were used to produce the mixtures, by heating and homogenization at 60 °C, in the PVA: CS volume ratios of 80:20, 70:30 and 60:40.

2.2.2. Rheological Characterization of Electrospinning Solutions

The rheological properties of the solutions were investigated at 25 °C within the linear viscoelastic range, at 6.28 rad·s⁻¹, on rheometer AR-G2 (TA Instruments, New Castle, DE, USA) using a concentric cylinder geometry. The variation of the storage modulus (G') and the loss modulus (G''), as a function of the oscillatory frequency, in the range from 0.1 to 100 rad·s⁻¹ was investigated.

2.2.3. Preparation of Electrospun and Crosslinked Mats

The environmental conditions used for electrospinning were 25 °C and 50% - 60% relative humidity. The prepared PVA:CS solutions were added to a 5 mL disposable syringe with a 0.55 mm internal diameter disposable needle (25G) with a KD Scientific Inc. pump, model 100 (Holliston, MA, USA) capable of maintaining solution injection flow controlled. A high voltage source (Series FC, Glassman High Voltage, Inc., USA), capable of providing a maximum potential difference of 60 kV, was attached to the tip of the metal needle, and a metal plate was connected to the ground wire and fixed to a certain distance from the needle tip. To produce crosslinked PVA:CS nanofibrous membranes, the samples were placed for 24 h in a vacuum desiccator containing 15 mL of 25% aqueous glutaraldehyde solution, maintained in a Petri dish. After crosslinking, extra glutaraldehyde was removed by placing the samples in a fume hood for 1 h; then, the samples were dried under vacuum for 24 h and 48 h.

2.2.4. Box-Behnken Design (BBD) of Electrospinning Process

Box-Behnken design was used to verify and identify the effect of 4 process parameters (applied voltage, solution flow, chitosan concentration in the mixture and distance between the needle and the collecting plate) on the mean fiber diameter (Y_1) and in the standard deviation of the fiber diameter (Y_2). In the present study, the four-factor, three-level Box-Behnken experimental design was applied to determine optimal conditions to minimize the mean diameter and standard deviation of nanofibers. Factor levels were coded as 1 (low), 0 (center point), and 1 (high) as shown in **Table 1**.

In a system involving four significant independent variables (X_1 , X_2 , X_3 and X_4), the mathematical relationship of the responses about these variables may be given approximately by the quadratic polynomial Equation (1).

$$Y = \beta_0 + \sum \beta_i X_i + \sum \beta_{ii} X_{ii}^2 + \sum \beta_{ij} X_i X_j + \varepsilon \quad (1)$$

Table 1. Actual values of the variables and their levels.

Coded variables	Input parameters	Levels		
		-1	0	1
X_1	Applied voltage (kV)	10	12.5	15
X_2	Flow rate (mL/h)	0.25	0.5	0.75
X_3	Chitosan (%)	20	30	40
X_4	Tip to needle distance (cm)	10	12.5	15

where β_0 is the offset term, β_i is the slope or linear effect of input factor X_i , β_{ii} is the quadratic effect of input factor X_i and β_{ij} is the linear-linear interaction effect between input factors X_i and X_j .

All experiments were performed in a random order to minimize the effect of unexpected variability on observed response due to external factors. Statistica 12.0 software was used for all statistical calculations.

2.2.5. Optimization of BBD by Desirability Function

Initially, each response (Y_1 and Y_2) was transformed into a dimensionless desirability function (d_i) within a range from 0 to 1 (the lowest and highest desirability). The value of d_i increases as the i -th response approaches the limits imposed. Equation (2) shows the global desirability index (D) obtained from the combined geometric means of the individual functions.

$$D = \left(d_1^{\alpha_1} \times d_2^{\alpha_2} \times d_3^{\alpha_3} \times \dots \times d_n^{\alpha_n} \right)^{1/n}, 0 \leq \alpha_i \leq 1 (i = 1, 2, 3, \dots, n), \sum_{i=1}^n \alpha_i = 1 \quad (2)$$

where d_i indicates the desirability of the different responses $Y_i (i = 1, 2, 3, \dots, n)$ and α represents the importance of the responses.

2.3. Water Stability

The nanofibers were soaked in distilled water and after 1 h they were carefully removed and dried with filter paper to remove surface water and then weighed. The materials were dried under vacuum to constant weight.

2.4. Characterization of PVA/CS Mats

The morphology of PVA/CS nanofibers was observed by scanning electron microscopy (SEM), using a Tescan model 212 Vega 3LMU (Brno-Kohoutovice, Czech Republic) equipment. The surfaces were vacuum coated with gold prior to measurements. SEM images were used to measure the average fiber diameters with the Size Meter Software. At least 50 nanofibers were randomly selected from each of the SEM images.

Structural characterization was performed by X-ray diffraction (XRD) operated with $\text{CuK}\alpha$ radiation ($\lambda = 0.15418$ nm). XRD analyses were performed in an Ultima IV diffractometer (Rigaku Corporation, Osaka, Japan) operating at the $\text{CuK}\alpha$ wavelength of 1.5418 \AA , at 40 kV and 20 mA. The scattered radiation was detected at ambient temperature in the 0.6° to 80° (2θ) angular region at 0.5°

(2θ)/min in the reflection mode. For a better visualization of the characteristic reflections, the diffractograms were smoothed using the software OriginPro 8.0 (Savitsky-Golay, polynome: 2, points of window: 10). The free software Fityk, downloaded at <http://www.unipress.waw.pl/fityk>, was used to determine the degree of crystallinity.

Infrared spectroscopy (FTIR) analyses were carried from 4000 cm^{-1} to 600 cm^{-1} , at ambient temperature, using a Perkin Elmer Frontier spectrometer (Waltham, MA, USA), equipped with an attenuated total reflection accessory (ATR), by averaging 60 scans with a resolution of 4 cm^{-1} in transmission mode.

Dynamic mechanical analyses (DMA) were performed in a Q800 DMA from TA Instruments, equipped with an accessory to measure tensile properties of mats with $(13.0 \pm 0.2)\text{ mm} \times (6.0 \pm 0.02)\text{ mm} \times (0.09 \pm 0.006)\text{ mm}$. The dynamic experiments were carried out at 1 Hz in the tensile mode, from -60°C to 310°C , at a heating rate of $3^\circ\text{C}/\text{min}$, after conditioning the samples at 25°C and 50% relative humidity, for a period of at least 48 h. Uniaxial tensile tests were performed in the same Q800 equipment, at 25°C , by the controlled force method under a force ramp of 1 N/min to 18 N up to the break of the sample. The average value was taken from a total of three measurements.

3. Results and Discussions

3.1. Development of Nanofibers

The combined effects of the independent variables (applied voltage, polymeric solution flow rate, chitosan concentration in the mixture and distance between plate and needle) on nanofiber diameter and homogeneity were evaluated by Box-Behnken design. According to statistical theory, a Box-Behnken design with four independent factors comprises 27 experiments as shown in **Table 2**, which also included coded variables and experimental and predicted values. The observed mean diameter (Y_1) and standard deviation (Y_2) values for PVA/CS nanofibers were in the range 186.6 - 354.2 nm and 27 - 139.7 nm, respectively, depending on the variation of conditions. The results were then evaluated by an ANOVA test to verify the significance of the independent variables, as well as their possible interactions, in order to obtain a mathematical model. The effect of each of the responses as well as their respective estimated coefficients and p values were compiled in **Table 3**. The p -value was used as a measure of statistical significance to assess the impact of each factor on the response, where p values greater than 0.05 do not significantly affect response within a confidence interval greater than 95%. Also, the lower the p -value, the more important that factor would be. For both responses, voltage was the factor with the greatest impact, followed by the distance between the plates and the chitosan concentration.

The insignificant coefficients ($p > 0.05$) were taken from the complete quadratic model in order to obtain a more refined mathematical model, and again through an ANOVA test, the coefficients were recalculated. The reduced response surface model for the mean diameter (Y_1) containing only statistically

Table 2. Box-Behnken 24 Experimental Matrix and the experimental and predicted Mean Fiber Diameter (nm) values and standard deviation of PVA:CS nanofibers.

Design Point	Coded levels of factor				Mean fiber diameter (nm) \pm Standard deviation (nm)	
	X_1	X_2	X_3	X_4	Experimental	Predicted
1	-1	-1	0	0	248.3 \pm 73.3	272.7 \pm 86.4
2	1	-1	0	0	197.6 \pm 38.7	192.4 \pm 44.2
3	-1	1	0	0	222.6 \pm 84.2	254.5 \pm 88.6
4	1	1	0	0	187.1 \pm 31.8	189.4 \pm 28.6
5	0	0	-1	-1	256.4 \pm 29.3	262.5 \pm 30.4
6	0	0	1	-1	209.2 \pm 49.5	211.8 \pm 53.0
7	0	0	-1	1	285.3 \pm 52.6	309.4 \pm 59.0
8	0	0	1	1	243.2 \pm 60.8	263.9 \pm 69.6
9 (C)	0	0	0	0	197.7 \pm 37.2	205.2 \pm 32.6
10	-1	0	0	-1	212.7 \pm 34.6	218.2 \pm 47.5
11	1	0	0	-1	186.8 \pm 39.1	203.7 \pm 37.0
12	-1	0	0	1	354.2 \pm 115.4	325.9 \pm 110.7
13	1	0	0	1	211.9 \pm 38.7	195.0 \pm 19.0
14	0	-1	-1	0	302.0 \pm 79.3	274.7 \pm 63.4
15	0	1	-1	0	274.7 \pm 35.5	280.2 \pm 42.9
16	0	-1	1	0	259.7 \pm 80.6	242.8 \pm 66.2
17	0	1	1	0	200.2 \pm 64.1	216.0 \pm 73.2
18 (C)	0	0	0	0	213.0 \pm 27.0	205.2 \pm 32.6
19	-1	0	-1	0	327.5 \pm 84.3	314.1 \pm 73.4
20	1	0	-1	0	278.4 \pm 45.6	283.3 \pm 57.3
21	-1	0	1	0	328.2 \pm 139.7	308.0 \pm 124.9
22	1	0	1	0	195.3 \pm 31.0	193.3 \pm 38.8
23	0	-1	0	-1	191.9 \pm 35.7	196.5 \pm 35.4
24	0	1	0	-1	218.7 \pm 39.7	183.0 \pm 24.7
25	0	-1	0	1	222.7 \pm 42.1	243.1 \pm 54.1
26	0	1	0	1	255.2 \pm 53.9	235.3 \pm 51.2
27 (C)	0	0	0	0	204.8 \pm 33.5	205.2 \pm 32.6

Table 3. Effect of independent variables and their estimated coefficients obtained for responses assessed by Box-Behnken planning. * ($R^2 = 85.92\%$, R^2 ajust = 69.50%) ** ($R^2 = 87.48\%$, R^2 ajust = 72.88%).

Factor	Term	Mean Fiber Diameter (nm)*			Standard Deviation (nm)**		
		Effect	p-value	Coefficient	Effect	p-value	Coefficient
Global Mean	β_0	257.71	0.0001	257.71	65.77	0.0007	65.77
X_1	β_1	-72.73	0.003	-36.36	-51.10	0.003	-25.55

Continued

X_1^2	β_{11}	-21.66	0.022	-10.83	-20.79	0.011	-10.39
X_2	β_2	-10.61	0.138	-5.31	-6.78	0.151	-3.39
X_2^2	β_{22}	-0.42	0.908	-0.21	-8.58	0.062	-4.29
X_3	β_3	-48.08	0.008	-24.04	16.55	0.031	8.27
X_3^2	β_{33}	-47.85	0.004	-23.93	-20.26	0.012	-10.12
X_3	β_4	49.46	0.007	24.73	22.60	0.016	11.30
X_3^2	β_{44}	-8.86	0.115	-4.43	-0.17	0.946	-0.08
X_1X_2	β_{12}	7.60	0.425	3.80	-8.90	0.226	-4.45
X_1X_3	β_{13}	-41.90	0.031	-20.95	-35.00	0.021	-17.50
X_1X_4	β_{14}	-58.20	0.016	-29.10	-40.60	0.015	-20.30
X_2X_3	β_{23}	-16.10	0.170	-8.05	13.75	0.116	6.87
X_2X_4	β_{24}	2.85	0.745	1.42	3.90	0.528	1.95
X_3X_4	β_{34}	2.55	0.770	1.28	-6.00	0.365	-3.00

significant terms within a 95% confidence interval ($p \leq 0.05$) is presented in Equation (3).

$$Y_1 = 254.61 - 36.37X_1 - 9.67X_1^2 - 24.04X_3 - 22.76X_3^2 + 24.73X_4 - 20.95X_1X_3 - 29.1X_1X_4 \quad (3)$$

where X_1 is the applied voltage (kV), X_3 is the concentration of chitosan solution in the mixture (%) and X_4 is the distance between the collecting plate and the needle.

The mathematical model for nanofiber standard deviation (Y_2) after the elimination of insignificant terms is presented in Equation (4).

$$Y_2 = 62.85 - 25.55X_1 - 9.30X_1^2 + 8.27X_3 - 9.03X_3^2 + 11.3X_4 - 17.5X_1X_3 - 20.3X_1X_4 \quad (4)$$

The p -value was also used to measure the statistical significance related to estimated coefficients of the presented models. It was observed that the equations obtained for the responses Y_1 (mean diameter) and Y_2 (standard deviation) were considered significant, with no lack of fit in reduced models. The p -value observed for mean diameter and standard deviation in reduced models was 0.1014 and 0.1256, respectively.

The adequacy of the predicted values by the model with the experimental data was also confirmed by the analysis of the coefficient of determination (R^2), which represents the proportion of the total variability that can be explained by a regression model. After excluding non-significant terms, the calculated value of R^2 was 0.84002 for the average diameter model, indicating that the model can explain 84% of the average diameter variation of nanofibers. The standard deviation model can explain 83% of the variation in the experimental observations. The adjusted R^2 value for the mean diameter (0.781) and standard deviation

(0.7677), after withdrawal of insignificant terms also showed a good correlation between the observed and predicted values, showing that the quadratic models obtained are significant and favorable for the representation of the relationship between the response and the independent variables.

3.2. Assessing 3D Surface Plots

Figures 1(a)-(d) show the estimated three-dimensional (3D) surface plots for the evaluated responses as a function of the selected independent parameters (two-factors-at-a-time) illustrating their relationships. The impact of the electrospinning parameters on fiber diameter and their homogeneity was assessed by 3D surface plots.

The influence of applied voltage on fiber diameter and their standard deviation was illustrated in Figures 1(a)-(d). It may be observed that, in relation to mean diameter and standard deviation, keeping one or more factors constant, the increase in applied voltage led to a decrease in the responses, up to a threshold limit in some regions. High voltage created an electrically charged polymeric jet out of the needle, and the electric field formed with the collecting plate, reducing the drop. Overcoming the surface tension by voltage led to the formation of the Taylor cone at the capillary outlet, initiating the electrospinning process. Increasing the applied voltage causes an increase on strength of electric field and

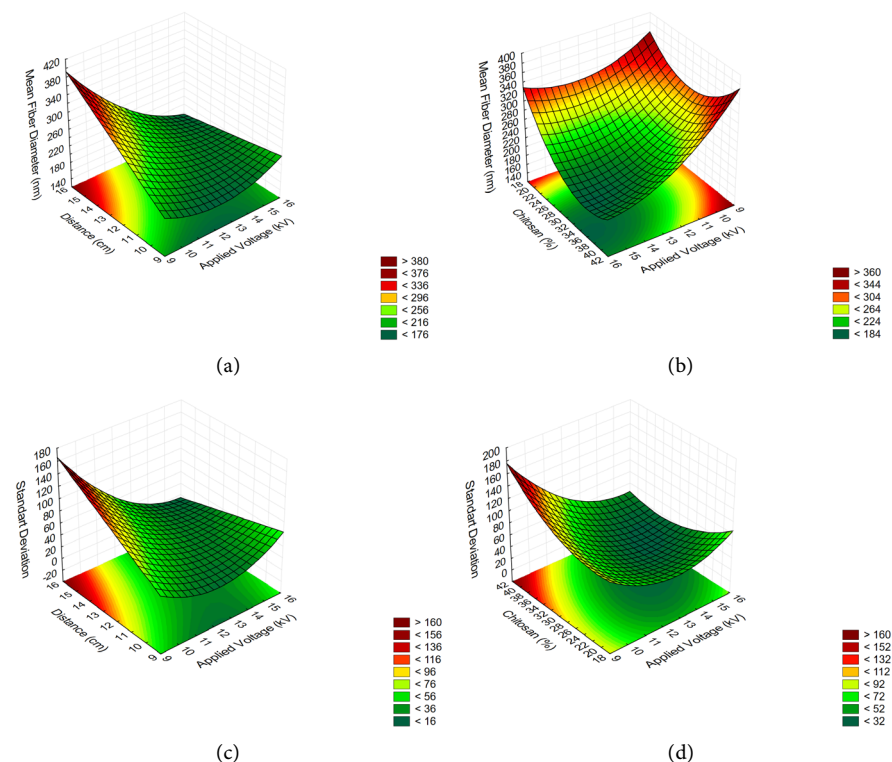


Figure 1. 3D surface plots for electrospinning parameters as a function of (a) applied voltage and distance tip-to-plate; (b) applied voltage and chitosan for mean fiber diameter; (c) applied voltage and distance tip-to-plate; (d) applied voltage and chitosan for standard deviation.

electrostatic stretching force leading to an accelerated jet, forming thinner nanofibers [2] [40] [41]. Also, it was possible to observe the curvature on the plots, which confirms the need for a quadratic regression model. The models show that applied voltage has significant interactions with tip-to-collector distance (X_1X_3) and chitosan content on blend (X_1X_4).

Figure 1(a) and **Figure 1(c)** shows the impact of tip-to-collector distance and applied voltage in nanofibers with flow rate and chitosan content kept constant at center point. A minimum distance was required to give the fibers enough time to evaporate the solvent before reaching the collecting plate, thus avoiding the appearance of failures if they are too close or too far away [42]. The impact of tip-to-plate distance is given by competition between long- and short-range effects. While shorter distances led to the formation of thinner fibers, due to increased electric field, longer distances provided longer jet stretching, due to longer flight times [43] [44].

Figure 1(b) and **Figure 1(d)** shows the effect of increasing chitosan concentration on PVA/CS mixture. As shown in **Figure 2(a)**, because of increased entanglements and intermolecular interactions between polymer molecules the solution viscosity was enhanced.

The liquid-like behavior of the solutions is shown in **Figure 2(b)**, in which the loss modulus (G'') is larger than the storage modulus (G') for all studied solutions. Thus, a higher voltage was required to charge the solutions and start the electrospinning process as shown in **Figure 1(b)**. It is possible to observe that in low voltage regions, regardless of the chitosan concentration, the average fiber diameter increased. However, the increase of the two factors caused a decrease in the responses, as already observed in the model, probably because of the significance of the term (X_1X_4).

3.3. Optimization of Nanofibers

The desirability function was used to optimize the influence of the production variables on the process of obtaining PVA/CS nanofibers, seeking to minimize the mean diameter and standard deviation. **Figure 3** shows the conditions

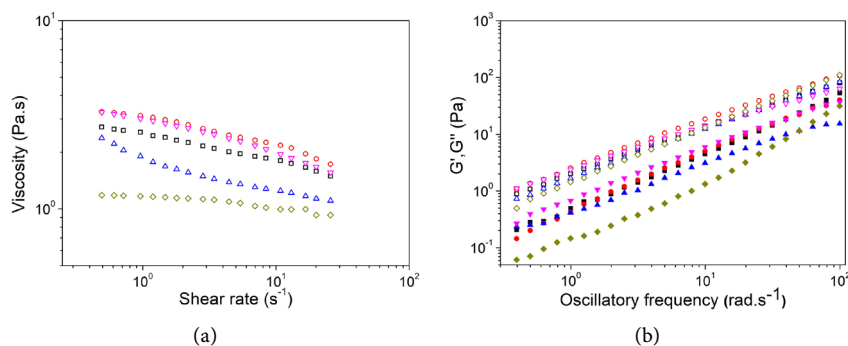


Figure 2. Viscosity versus shear rate at 25°C and 5% strain amplitude, for the electrospinning solutions of PVA/CS blends at 60:40 (\square), 70:30 (\circ), 80:20 (Δ) compositions, PVA 10% (\diamond) and chitosan 2.5% (∇) (a) and G' (open symbols) and G'' (full symbols) versus oscillation frequency at 25°C and 5% strain amplitude.

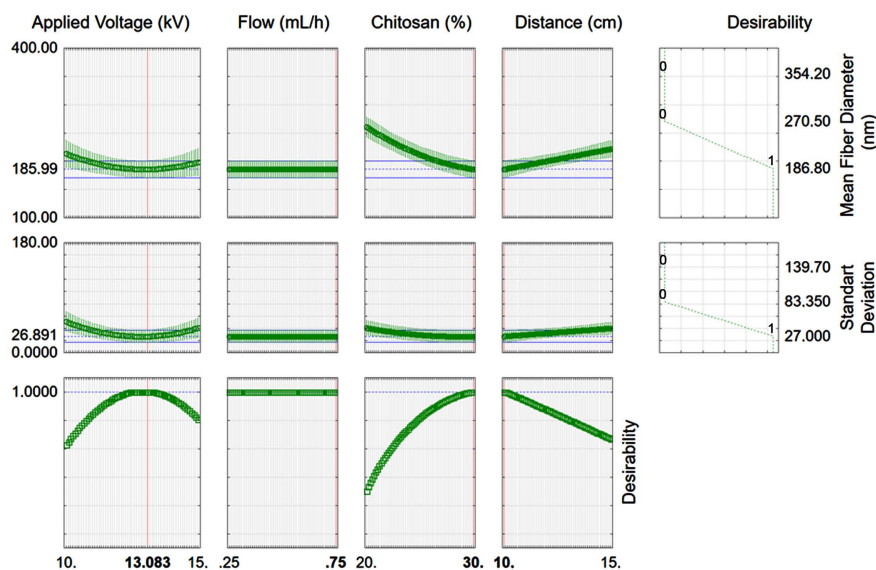


Figure 3. Profiles for predicted values of individual and global desirability in optimization of data generated using Box-Behnken design for mean fiber diameter and standard deviation of PVA/CS nanofibers.

obtained after the test application, in which the smallest diameter and standard deviation nanofibers were obtained by optimizing all independent variables. The conditions for lower mean fiber diameter and lower standard deviation by desirability function were Applied Voltage = 13.1 kV, Chitosan concentration = 30% and distance tip-to-plate = 10 cm. As the flow rate was not statistically significant, it was kept at the center point value (0.5 mL/h). The predicted values for mean fiber diameter and the standard deviation were calculated based on the obtained model. The observed values for mean fiber diameter and standard deviation were (196.5 ± 28.3) nm, compared to the predicted values of (185.9 ± 26.8) nm. The error was less than 5% and acceptable.

3.4. Stability of PVA/CS Mats in Water

Since PVA is water soluble, a simple contact with water can immediately destroy PVA/CS mats (**Figure 4(a)**) compromising their wound dressing application as shown in **Figure 4(b)**. A crosslink treatment was performed to guarantee water resistance, maintaining the nanofibrous structure with contact with water. After a 24 h treatment with GTA, water stability was increased. Glutaraldehyde treatment was able to increase stability in water, regardless of exposure time, as shown in **Figure 4(c)** and **Figure 4(e)**. After a 24 h treatment, it was possible to observe a decrease in nanofiber diameter to 126.5 ± 25.7 nm. A 35.5% reduction compared to fiber diameter without crosslinking. Regarding morphology, it can be observed that after 1 h of immersion, the fibrous morphology was not lost; however, there was swelling of the nanofibers with visible coalescence that prevented the correct measurement of the average diameter (**Figure 4(d)**). The 48 h treatment (**Figure 4(e)** and **Figure 4(f)**) showed an even larger diameter reduction, 44.8% (108.4 ± 15.4) nm, with fibers slightly altered after exposure to water,

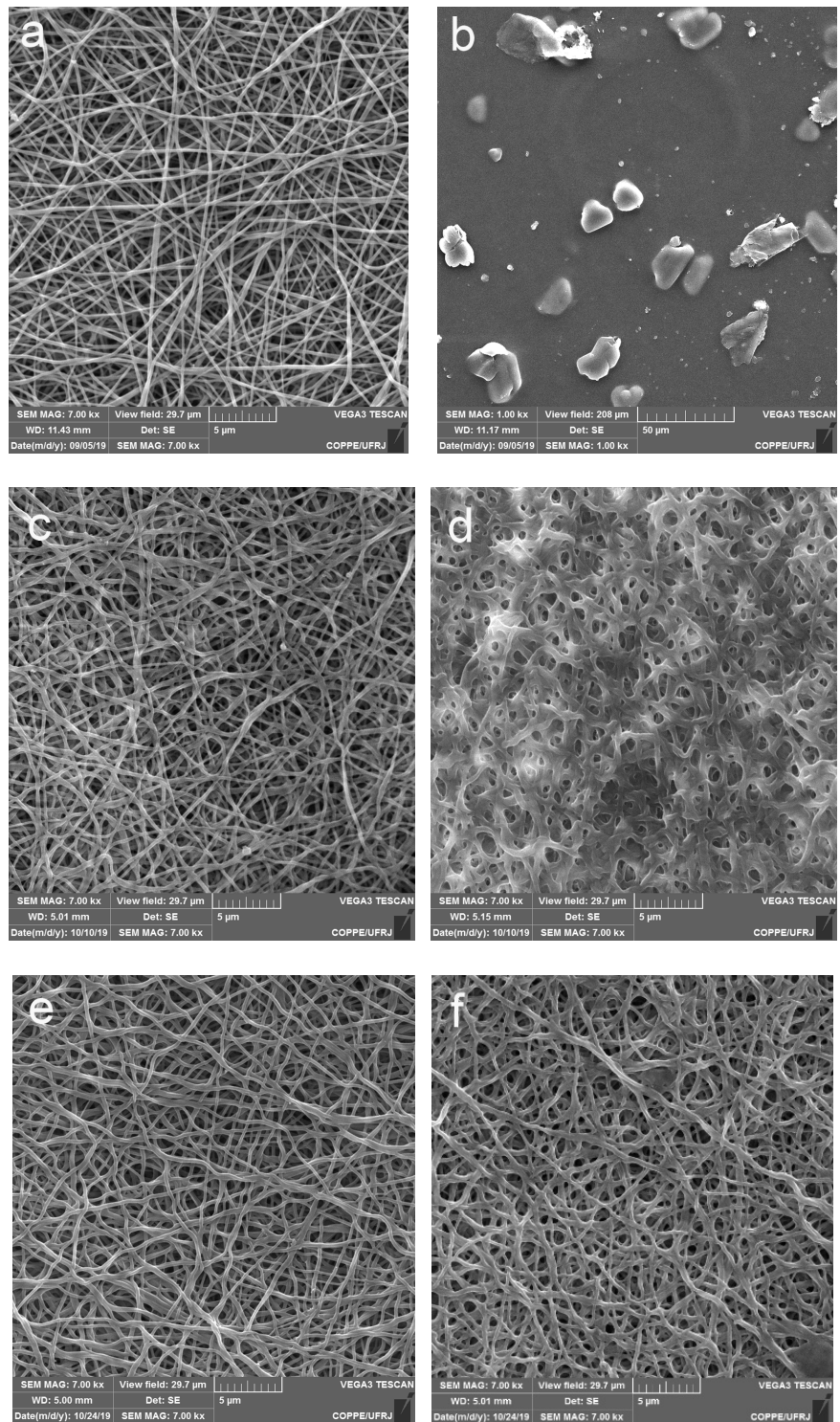


Figure 4. SEM images for PVA/CS fiber membranes: (a) uncrosslinked; (b) uncrosslinked after immersion in water for 1 h; (c) 24 h crosslinking; (d) 24 h crosslinking after immersion in water for 1 h; (e) 48 h crosslinking; (f) 48 h crosslinking after immersion in water for 1 h.

with an average diameter of (128.4 ± 22.4) nm, maintaining its homogeneous appearance, confirming the efficiency of the vapor-phase crosslinking reaction

by GTA.

3.5. Characterization of PVA/CS Mats

FTIR spectra were used to assess structural changes that occurred after crosslinking with GTA. **Figure 5(a)** shows the spectra before (trace I) and after crosslinking (trace II—24 h and trace III—48 h), and it is possible to observe that the position of most bands remained the same; only their intensities were changed. In trace I, the broad band observed in the range 3650 cm^{-1} to 3000 cm^{-1} resulted from O–H stretching of PVA and O–H and N–H stretching from CS. The two bands in the 3000 cm^{-1} to 2750 cm^{-1} range were attributed to asymmetrical and symmetrical C–H stretching. The band at $\sim 1740\text{ cm}^{-1}$ was assigned to C=O stretching of nonhydrolyzed vinyl acetate groups [45]. The absorptions at 1658 cm^{-1} and 1590 cm^{-1} may be attributed, respectively, to the amide I (C=O stretching) and amide II (C–N stretching and C–N–H bending vibrations) from CS. After exposure to GTA (trace II and trace III), competitive and parallel reactions may occur between GTA and hydroxyl and amine groups present in PVA and chitosan. The appearance of a doublet at the C–H region, as well as the increase in intensity of the band associated to C–H bending at $\sim 1459\text{ cm}^{-1}$ may be attributed to the introduced crosslinking agent in the chitosan phase, when a vapor phase GTA crosslinking procedure was applied [46] [47] [48] [49].

The crystallinity of uncrosslinked and crosslinked 70:30 PVA/CS mats were evaluated by X-ray diffraction (**Figure 5(b)**). According to the literature, the characteristic chitosan crystalline peaks are not visualized when the PVA composition is high in PVA/CS mats [46]. For the uncrosslinked mat (**Figure 5(b)**, trace I), the only maximum is in the $19^\circ - 20^\circ$ (2θ) region, and was related to the combined 101 and 200 reflections of semicrystalline PVA [50]. The intensity of this characteristic PVA reflection decreased significantly for the crosslinked mat (**Figure 5(b)**, trace II and III). Therefore, the degrees of crystallinity found were 22.5% for the uncrosslinked and 9.5% and 4.7% for the 24 h and 48 h crosslinked materials, respectively. This behavior is in accordance with the formation of crosslinks, which hinder the mobility of PVA molecules, and this phenomenon depends on the exposure time to GTA.

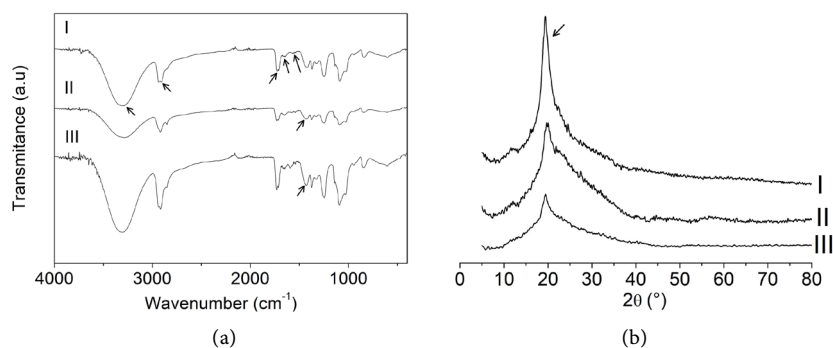


Figure 5. FT-IR spectra (a), XRD patterns (b) of PVA/CS mats before (Trace I) and after crosslinking for 24 h and 48 h (Trace II and III respectively).

3.6. Mechanical Behavior

Dynamic mechanical analyses were carried out for uncrosslinked and crosslinked optimized PVA/CS mats. The variation of the loss factor ($\tan\delta$), given by the ratio between loss modulus (E'') and storage modulus (E') values, as a function of temperature are shown in **Figure 6(a)**, within the -60°C to 310°C range. This factor is used as an indicator of stiffness or flexibility. In **Figure 6(a)**, the peak at 10.5°C , observed for the uncrosslinked sample, was attributed to the γ relaxation of CS. No significant change was observed for the 24 h crosslinked mat. The peak at 110.3°C , observed for the uncrosslinked mat may be attributed to the PVA α relaxation, associated with its dynamic glass transition temperature (T_g), and to encompass the β relaxation peak for CS [51]. At a higher temperature, the peak with its maximum at 201.8°C may be attributed to the α transition of CS. The presence of two α relaxations for the PVA/CS uncrosslinked mat revealed lack of miscibility between PVA and CS. On the other hand, for the crosslinked samples only one broad peak was observed in the $\sim 60^\circ\text{C}$ to 235°C temperature range for both crosslinked products. However, it is possible to observe a shift of the $\tan\delta$ peak with increasing exposure time to GTA. The increase in $\tan\delta$ observed for the product obtained after 48 h indicates a higher crosslinking density. In the crosslinked structure, a higher crosslinking density means a shorter distance between molecular chains. Such an arrangement forces the segments of the chains to be in a more intimate contact improving energy dissipation [52] [53].

Figure 6(b) shows the Tensile tests results for the mats. For the uncrosslinked mat, the lowest Young's modulus, $E = (153.5 \pm 12.8)$ MPa, and tensile stress at break, $\sigma_{\max} = (6.6 \pm 0.3)$ MPa are attributed to the brittle character of chitosan. However, the highest strain at break, $\varepsilon_{\max} = (10.1 \pm 1.3)\%$, is assigned to the flexibility of PVA chains of this PVA-richest composition. For the 24 h and 48 h crosslinked mats, enhanced properties were observed in both treatments and the results are summarized in **Table 4**. The decrease in elongation at break was assigned to the reduction in stretchiness after crosslinking reactions, which involved $-\text{OH}$ and $-\text{NH}_2$ groups of PVA and CS.

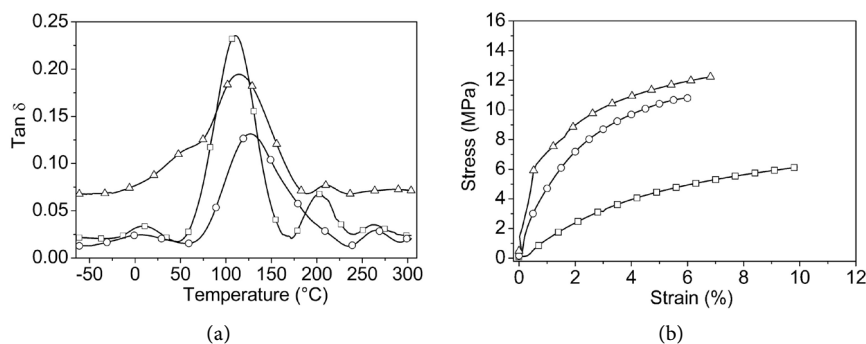


Figure 6. Tangent delta as a function of temperature (a) and stress versus strain curves (b) for PVA/CS optimized mats uncrosslinked (\square), 24 h crosslinked (\circ) and 48 h crosslinked (Δ) with GTA vapor.

Table 4. Mechanical properties determined for the products.

Sample	Young's modulus, E (MPa)	Strain at break, ϵ_{\max} (%)	Tensile stress at break, σ_{\max} (MPa)
Uncrosslinked	153.5 ± 12.8	10.1 ± 1.3	6.6 ± 0.3
Crosslinked—24 h	636.2 ± 12.1	4.3 ± 0.5	11.8 ± 1.0
Crosslinked—48 h	754.1 ± 9.4	6.9 ± 0.8	13.1 ± 0.9

4. Conclusion

In this study, PVA/CS nanofibers were fabricated. Process parameters and PVA/CS blend composition were optimized to determine their influence on the formation of small size nanofibers and good homogeneity, observed through standard deviation. A response surface methodology, combining Box-Behnken planning and desirability function, was employed to obtain and optimize a mathematical model for this system. A second order regression model was obtained and proved adequate to predict the behavior of PVA/CS fibers within the limits of the studied factors. The minimum diameter with minimum standard deviation was (196.5 ± 28.3) nm under conditions of 13.1 kV for applied voltage, 30% CS and 10 cm distance plate-to-tip. The flow rate was not significant for the studied limits. The optimized fibers were crosslinked and analyzed for stability in water, characterized by X-ray diffraction and Fourier transform infrared spectroscopy. The results revealed that 48 h exposure to the crosslinking agent (GTA vapor) was efficient to promote water stability and enhanced tensile strength. In this way, it was possible to optimize the electrospinning process and the water resistant PVA/CS of nanofibers, which enables the use of these materials as drug release systems.

Acknowledgements

The authors acknowledge Conselho Nacional de Desenvolvimento Científico e Tecnológico (CNPq) (Grant N° 141363/2017-0) for financial support.

Conflicts of Interest

The authors declare no competing interests.

References

- [1] Abid, S., Hussain, T., Raza, Z.A. and Nazir, A. (2019) Current Applications of Electrospun Polymeric Nanofibers in Cancer Therapy. *Materials Science and Engineering: C*, **97**, 966-977. <https://doi.org/10.1016/j.msec.2018.12.105>
- [2] Ngadiman, N.H., Yusof, N.M., Idris, A., Misran, E. and Kurniawana, D. (2017) Development of Highly Porous Biodegradable γ -Fe₂O₃/Polyvinyl Alcohol Nanofiber Mats Using Electrospinning Process for Biomedical Application. *Materials Science and Engineering: C*, **70**, 520-534. <https://doi.org/10.1016/j.msec.2016.09.002>
- [3] Chahal, S., Kumar, A. and Hussian, F.S.J. (2019) Development of Biomimetic Electrospun Polymeric Biomaterials for Bone Tissue Engineering: A Review. *Journal of Biomaterials Science, Polymer Edition*, **30**, 1308-1355.

- <https://doi.org/10.1080/09205063.2019.1630699>
- [4] Cui, W.G., Zhou, Y. and Chang, J. (2010) Electrospun Nanofibrous Materials for Tissue Engineering and Drug Delivery. *Science and Technology of Advanced Materials*, **11**, 1-11. <https://doi.org/10.1088/1468-6996/11/1/014108>
- [5] Ambekar, R.S. and Kandasubramanian, B. (2019) Progress in the Advancement of Porous Biopolymer Scaffold: Tissue Engineering Application. *Industrial & Engineering Chemistry Research*, **58**, 6163-6194. <https://doi.org/10.1021/acs.iecr.8b05334>
- [6] Massella, D., Argenziano, M., Ferri, A., Guan, J., Giraud, S., Cavalli, R., Barresi, A.A. and Salaün, F. (2019) Bio-Functional Textiles: Combining Pharmaceutical Nano-carriers with Fibrous Materials for Innovative Dermatological Therapies. *Pharmaceutics*, **11**, 1-29. <https://doi.org/10.3390/pharmaceutics11080403>
- [7] Nakielski, P. and Pierini, F. (2019) Blood Interactions with Nano- and Microfibers: Recent Advances, Challenges and Applications in Nano- and Microfibrous Hemostatic Agents. *Acta Biomaterialia*, **84**, 63-76. <https://doi.org/10.1016/j.actbio.2018.11.029>
- [8] Barnes, C.P., Sell, S.A., Boland, E.D., Simpson, D.G. and Bowlin, G.L. (2007) Nanofiber Technology: Designing the Next Generation of Tissue Engineering Scaffolds. *Advanced Drug Delivery Reviews*, **59**, 1413-1433. <https://doi.org/10.1016/j.addr.2007.04.022>
- [9] Chew, S.Y., Wen, Y., Dzenis, Y. and Leong, K.W. (2006) The Role of Electrospinning in the Emerging Field of Nanomedicine. *Current Pharmaceutical Design*, **12**, 4751-4770. <https://doi.org/10.2174/138161206779026326>
- [10] Qasim, S.B., Zafar, M.S., Najeeb, S., Khurshid, Z., Shah, A.H., Husain, S. and Rehman, I.U. (2018) Electrospinning of Chitosan-Based Solutions for Tissue Engineering and Regenerative Medicine. *International Journal of Molecular Sciences*, **19**, 1-26. <https://doi.org/10.3390/ijms19020407>
- [11] Ali, A. and Ahmed, S. (2018) A Review on Chitosan and Its Nanocomposites in Drug Delivery. *International Journal of Biological Macromolecules*, **109**, 273-286. <https://doi.org/10.1016/j.ijbiomac.2017.12.078>
- [12] Levengood, S.K.L. and Zhang, M. (2014) Chitosan-Based Scaffolds for Bone Tissue Engineering. *Journal of Materials Chemistry B*, **2**, 3161-3184. <https://doi.org/10.1039/c4tb00027g>
- [13] Luque-Alcaraz, A., Lizardi-Mendoza, J., Goycoolea, F., Higuera-Ciapara, I. and Argüelles-Monal, W. (2016) Preparation of Chitosan Nanoparticles by Nanoprecipitation and Their Ability as a Drug Nanocarrier. *RSC Advances*, **6**, 59250-59256. <https://doi.org/10.1039/C6RA06563E>
- [14] Sanyakamdhorn, S., Agudelo, D. and Tajmir-Riahi, H. (2013) Encapsulation of Antitumor Drug Doxorubicin and Its Analogue by Chitosan Nanoparticles. *Biomacromolecules*, **14**, 557-563. <https://doi.org/10.1021/bm3018577>
- [15] Katas, H., Raja, M.A.G. and Lam, K.L. (2013) Development of Chitosan Nanoparticles as a Stable Drug Delivery System for Protein/siRNA. *International Journal of Biomaterials*, **2013**, Article ID: 146320. <https://doi.org/10.1155/2013/146320>
- [16] Ardeshirzadeh, B., Anaraki, N.A., Irani, M., Rad, L.R. and Shamshiri, S. (2015) Controlled Release of Doxorubicin from Electrospun PEO/Chitosan/Graphene Oxide Nanocomposite Nanofibrous Scaffolds. *Materials Science and Engineering: C*, **48**, 384-390. <https://doi.org/10.1016/j.msec.2014.12.039>
- [17] Mirzaei, E., Sarkar, S., Rezayat, S.M. and Faridi-Majidi, R. (2016) Herbal Extract Loaded Chitosan-Based Nanofibers as a Potential Wound-Dressing. *JAMSAT*, **2**,

- 141-150. <https://doi.org/10.18869/nrip.jamsat.2.1.141>
- [18] Frohbergh, M.E., Katsman, A., Botta, G.P., Lazarovici, P., Schauer, C.L., Wegst, U.G.K. and Lelkes, P.I. (2012) Electrospun Hydroxyapatite-Containing Chitosan Nanofibers Crosslinked with Genipin for Bone Tissue Engineering. *Biomaterials*, **33**, 9167-9178. <https://doi.org/10.1016/j.biomaterials.2012.09.009>
- [19] Silva, M.A., Crawford, A., Mundy, J.M., Correlo, V.M., Sol, P., Bhattacharya, M., Hatton, P.V., Reis, R.L. and Neves, N.M. (2010) Chitosan/Polyester-Based Scaffolds for Cartilage Tissue Engineering: Assessment of Extracellular Matrix Formation. *Acta Biomaterialia*, **6**, 1149-1157. <https://doi.org/10.1016/j.actbio.2009.09.006>
- [20] Garcia-Cruz, D.M., Gomes, M., Reis, R.L., Moratal, D., Salmerón-Sánchez, M., Ribelles, J.L. and Mano, J.F. (2010) Differentiation of Mesenchymal Stem Cells in Chitosan Scaffolds with Double Micro and Macroporosity. *Journal of Biomedical Materials Research A*, **95**, 1182-1193. <https://doi.org/10.1002/jbm.a.32906>
- [21] Oliveira, J., Crawford, A., Mundy, J.L., Sol, P., Correlo, V.M., Bhattacharya, M., Neves, N.M., Hatton, P.V. and Reis, R.L. (2011) Novel Melt-Processable Chitosan-Polybutylene Succinate Fibre Scaffolds for Cartilage Tissue Engineering. *Journal of Biomaterials Science, Polymer Edition*, **22**, 773-788. <https://doi.org/10.1163/092050610X494604>
- [22] Fadaie, M., Mirzaei, E., Asvar, Z. and Azarpira, N. (2019) Stabilization of Chitosan Based Electrospun Nanofibers through a Simple and Safe Method. *Materials Science and Engineering. C*, **98**, 369-380. <https://doi.org/10.1016/j.msec.2018.12.133>
- [23] Zheng, H., Du, Y., Yu, J., Huang, R. and Zhang, L. (2001) Preparation and Characterization of Chitosan/Poly(Vinyl Alcohol) Blend Fibers. *Journal of Applied Polymer Science*, **80**, 2558-2565. <https://doi.org/10.1002/app.1365>
- [24] Merlusca, I.P., Matitut, D.S., Lisa, G., Sillion, M., Gradinaru, L., Oprea, S. and Popa, I.M. (2018) Preparation and Characterization of Chitosan-Poly(Vinyl Alcohol)-Neomycin Sulfate Films. *Polymer Bulletin*, **75**, 3971-3986. <https://doi.org/10.1007/s00289-017-2246-1>
- [25] Wei, Y., Zhang, X., Song, Y., Han, B., Hu, X., Wang, X., Lin, Y. and Deng, X. (2001) Magnetic Biodegradable Fe₃O₄/CS/PVA Nanofibrous Membranes for Bone Regeneration. *Biomedical Materials*, **6**, Article ID: 055008. <https://doi.org/10.1088/1748-6041/6/5/055008>
- [26] Jannesari, M., Varshosaz, J., Morshed, M. and Zamani, M. (2011) Composite Poly(Vinyl Alcohol)/Poly(Vinyl Acetate) Electrospun Nanofibrous Mats as a Novel Wound Dressing Matrix for Controlled Release of Drugs. *International Journal of Nanomedicine*, **6**, 993-1003. <https://doi.org/10.2147/IJN.S17595>
- [27] Hoffman, A.S. (2012) Hydrogels for Biomedical Applications. *Advanced Drug Delivery Reviews*, **64**, 18-23. <https://doi.org/10.1016/j.addr.2012.09.010>
- [28] Bas, D. and Boyac, I.H. (2007) Modeling and Optimization I: Usability of Response Surface Methodology. *Journal of Food Engineering*, **78**, 836-845. <https://doi.org/10.1016/j.jfoodeng.2005.11.024>
- [29] Ferreira, S.L.C., Bruns, R.E. and Ferreira, H.S. (2007) Box-Behnken Design: An Alternative for the Optimization of Analytical Methods. *Analytica Chimica Acta*, **597**, 179-186. <https://doi.org/10.1016/j.aca.2007.07.011>
- [30] Maran, J.P., Manikandan, S., Thirugnanasambandham, K., Nivetha, C.V. and Dinsh, R. (2013) Box-Behnken Design Based Statistical Modeling for Ultrasound-Assisted Extraction of Corn Silk Polysaccharide. *Carbohydrate Polymers*, **92**, 604-611. <https://doi.org/10.1016/j.carbpol.2012.09.020>
- [31] Roosta, M., Ghaedi, M. and Daneshfar, A. (2014) Optimization of Ultrasound-Assisted

- Reverse Micelles Dispersive Liquid-Liquid Micro-Extraction by Box-Behnken Design for Determination of Acetoin in Butter Followed by High Performance Liquid Chromatography. *Food Chemistry*, **161**, 120-126.
<https://doi.org/10.1016/j.foodchem.2014.03.043>
- [32] Gönen, S.O., Taygun, M.E., Aktürk, A. and Küçükbayrak, S. (2016) Fabrication of Nanocomposite Mat through Incorporating Bioactive Glass Particles into Gelatin/Poly(ϵ -Caprolactone) Nanofibers by Using Box-Behnken Design. *Materials Science and Engineering: C*, **67**, 684-693. <https://doi.org/10.1016/j.msec.2016.05.065>
- [33] Lou, H., Li, W., Li, C. and Wang, X. (2013) Systematic Investigation on Parameters of Solution Blown Micro/Nanofibers Using Response Surface Methodology Based on Box-Behnken Design. *Journal of Applied Polymer Science*, **130**, 1383-1391.
<https://doi.org/10.1002/app.39317>
- [34] Dalvand, K. and Ghiasvand, A. (2019) Simultaneous Analysis of PAHs and BTEX in Soil by a Needle Trap Device Coupled with GC-FID and Using Response Surface Methodology Involving Box-Behnken Design. *Analytica Chimica Acta*, **1083**, 119-129.
<https://doi.org/10.1016/j.aca.2019.07.063>
- [35] Abbasi, A., Nasef, N.M., Faridi-Majidi, R., Etesami, M., Takeshi, M. and Abouzar-Lotf, E. (2018) Highly Flexible Method for Fabrication of Poly(Glycidyl Methacrylate) Grafted Polyolefin Nanofiber. *Radiation Physics and Chemistry*, **151**, 283-291.
<https://doi.org/10.1016/j.radphyschem.2018.07.002>
- [36] Gönen, S.O., Taygun, M.E. and Küçükbayrak, S. (2016) Evaluation of the Factors Influencing the Resultant Diameter of the Electrospun Gelatin/Sodium Alginate Nanofibers via Box-Behnken Design. *Materials Science and Engineering: C*, **58**, 709-723. <https://doi.org/10.1016/j.msec.2015.09.024>
- [37] Zhu, C. and Liu, X. (2013) Optimization of Extraction Process of Crude Polysaccharides from Pomegranate Peel by Response Surface Methodology. *Carbohydrate Polymers*, **92**, 1197-1202. <https://doi.org/10.1016/j.carbpol.2012.10.073>
- [38] Wang, J. and Wan, W. (2009) Application of Desirability Function Based on Neural Network for Optimizing Biohydrogen Production Process. *International Journal of Hydrogen Energy*, **34**, 1253-1259. <https://doi.org/10.1016/j.ijhydene.2008.11.055>
- [39] Derringer, G. and Suich, R. (1980) Simultaneous Optimization of Several Response Variables. *Journal of Quality Technology*, **12**, 214-219.
<https://doi.org/10.1080/00224065.1980.11980968>
- [40] Li, D. and Younan, X. (2004) Direct Fabrication of Composite and Ceramic Hollow Nanofibers by Electrospinning. *Nano Letters*, **4**, 933-938.
<https://doi.org/10.1021/nl049590f>
- [41] Kulkarni, A., Bambole, V.A. and Mahanwar, P.A. (2010) Electrospinning of Polymers, Their Modeling and Applications. *Polymer-Plastics Technology and Engineering*, **49**, 427-441. <https://doi.org/10.1080/03602550903414019>
- [42] Bhardwaj, N. and Kundu, S.C. (2010) Electrospinning: A Fascinating Fiber Fabrication Technique. *Biotechnology Advances*, **28**, 325-347.
<https://doi.org/10.1016/j.biotechadv.2010.01.004>
- [43] Neo, Y.P., Ray, S., Easteal, A.J., Nikolaidis, M.G. and Quek, S.Y. (2012) Influence of Solution and Processing Parameters towards the Fabrication of Electrospun Zein Fibers with Sub-Micron Diameter. *Journal of Food Engineering*, **109**, 645-651.
<https://doi.org/10.1016/j.jfoodeng.2011.11.032>
- [44] Li, L., Jiang, Z., Xu, J. and Fang, T. (2014) Predicting Poly(Vinyl Pyrrolidone)'s Solubility Parameter and Systematic Investigation of the Parameters of Electrospinning with Response Surface Methodology. *Journal of Applied Polymer Science*, **131**,

40304. <https://doi.org/10.1002/app.40304>
- [45] Wu, Y., Ying, Y., Liu, Y., Zhang, H. and Huang, J. (2018) Preparation of Chitosan/Poly Vinyl Alcohol Films and Their Inhibition of Biofilm Formation against *Pseudomonas aeruginosa* PAO1. *International Journal of Biological Macromolecules*, **118**, 2131-2137. <https://doi.org/10.1016/j.ijbiomac.2018.07.061>
- [46] Jia, Y., Gong, J., Gu, X., Kim, H., Dong, J. and Shen, X. (2007) Fabrication and Characterization of Poly(Vinyl Alcohol)/Chitosan Blend Nanofibers Produced by Electrospinning Method. *Carbohydrate Polymers*, **67**, 403-409. <https://doi.org/10.1016/j.carbpol.2006.06.010>
- [47] Mansur, H.S., Costa, E.S., Mansur, A.A.P. and Barbosa-Stancioli, E.F. (2009) Cytocompatibility Evaluation in Cell-Culture Systems of Chemically Crosslinked Chitosan/PVA Hydrogels. *Materials Science and Engineering: C*, **29**, 1574-1583. <https://doi.org/10.1016/j.msec.2008.12.012>
- [48] Roy, S., Das, T., Kuddannaya, S. and Kim, J.W. (2017) A Novel Approach of Fabricating Highly Tunable and Fluffy Bioinspired 3D Poly(Vinyl Alcohol) (PVA) Fiber Scaffolds. *Nanoscale*, **9**, 7081-7093. <https://doi.org/10.1039/C7NR00503B>
- [49] Destaye, A.G., Lin, C.K. and Lee, C.K. (2013) Glutaraldehyde Vapor Crosslinked Nanofibrous PVA Mat with *in Situ* Formed Silver Nanoparticles. *ACS Applied Materials & Interfaces*, **5**, 4745-4752. <https://doi.org/10.1021/am401730x>
- [50] Lu, L., Peng, F., Jiang, Z. and Wang, J. (2006) Poly(Vinyl Alcohol)/Chitosan Blend Membranes for Pervaporation of Benzene/Cyclohexane Mixtures. *Journal of Applied Polymer Science*, **101**, 167-173. <https://doi.org/10.1002/app.23158>
- [51] Pereira, P.F. and Andrade, C.T. (2017) Optimized pH-Responsive Film Based on a Eutectic Mixture-Plasticized Chitosan. *Carbohydrate Polymers*, **165**, 238-246. <https://doi.org/10.1016/j.carbpol.2017.02.047>
- [52] Lei, Y., Zhou, S., Zou, H. and Liang, M. (2019) Effect of Crosslinking Density on Resilient Performance of Low-Resilience Flexible Polyurethane Foams. *Polymer Engineering & Science*, **55**, 308-315. <https://doi.org/10.1002/pen.23888>
- [53] Khorshidi, S., Solouk, A., Karkhaneh, A., Mirzadeh, H., Sharifi, S. and Mazinani, S. (2016) Effect of Crosslinking Procedure on Structural, Thermal, and Functional Performances of Cellulosic Nanofibers: A Comparison between Chemical and Photochemical Crosslinking. Mixtures. *Journal of Applied Polymer Science*, **133**, Article No. 43832. <https://doi.org/10.1002/app.43832>